



Swansea University
Prifysgol Abertawe



Cronfa - Swansea University Open Access Repository

This is an author produced version of a paper published in:

Applied Physics Letters

Cronfa URL for this paper:

<http://cronfa.swan.ac.uk/Record/cronfa34847>

Paper:

Lu, C., Li, X., Tang, L., Lai, S., Rogée, L., Teng, K., Qian, F., Zhou, L. & Lau, S. (2017). Tellurium quantum dots: Preparation and optical properties. *Applied Physics Letters*, 111(6), 063112

<http://dx.doi.org/10.1063/1.4993819>

This item is brought to you by Swansea University. Any person downloading material is agreeing to abide by the terms of the repository licence. Copies of full text items may be used or reproduced in any format or medium, without prior permission for personal research or study, educational or non-commercial purposes only. The copyright for any work remains with the original author unless otherwise specified. The full-text must not be sold in any format or medium without the formal permission of the copyright holder.

Permission for multiple reproductions should be obtained from the original author.

Authors are personally responsible for adhering to copyright and publisher restrictions when uploading content to the repository.

<http://www.swansea.ac.uk/iss/researchsupport/cronfa-support/>

Tellurium Quantum Dots: Preparation, and Optical Properties

Chaoyu Lu,¹ Xueming Li,^{1,a)} Libin Tang,^{2,b)} Sin Ki Lai,³ Lukas Rogée,³ Kar Seng Teng,⁴ Fuli Qian,¹ Liangliang Zhou,¹ and Shu Ping Lau³

¹ *Key Laboratory of Advanced Technique & Preparation for Renewable Energy Materials, Ministry of Education, Yunnan Normal University, Kunming, 650500, P. R. China*

² *Kunming Institute of Physics, Kunming 650223, P. R. China*

³ *Department of Applied Physics, The Hong Kong Polytechnic University, Hong Kong SAR, P. R. China*

⁴ *College of Engineering, Swansea University, Bay Campus, Fabian Way, Swansea SA1 8EN, United Kingdom*

1. Abstract

Herein we report an effective and simple method for producing Tellurium Quantum dots (TeQDs), a zero-dimensional nanomaterial with great prospects for biomedical applications. Their preparation is based on the ultrasonic exfoliation of Te powder dispersed in 1-methyl-2-pyrrolidone. The sonication causes the van der Waals forces between the structural hexagons of Te to break, so that the relatively coarse powder breaks down into nanoscale particles. The TeQDs have an average size of about 4 nm. UV-Vis absorption spectra of the TeQDs showed an absorption peak at 288 nm. Photoluminescence excitation (PLE) and photoluminescence (PL) study the optical properties of TeQDs. Both the PLE and PL peaks revealed a linear relationship against the emission and excitation energies respectively. TeQDs show important potential applications in biological imaging and catalysts as well as optoelectronics.

2. Introduction

Since the discovery of low-dimensional materials, extensive studies have shown that the properties of these materials altered significantly when they are in nanoscale regime. For example, a low-dimensional material can exhibit unique mechanical, electrical or optical properties that are different from those of their bulk counterparts. Quantum dots (QDs), the lowest-dimensional materials, are no exception to that and they could be engineered to display a wide range of properties that appear attractive for many modern fields of study.

^{a)} E-mail: lxmscience@163.com

^{b)} E-mail: scitang@163.com

Quantum dots (QDs) with diameter typically smaller than 10 nm have attracted much research interests in recent years due to their possible applications in biomedicine, such as photothermal therapy for cancer cell ablation and bioimaging.¹⁻⁴ The optical properties of QDs are indispensable factors in deciding over their suitability for these applications.⁵⁻⁷ For example, lasers with a wavelength of ~ 800 nm are commonly used in photothermal therapy as it allows penetration of the biological tissues, such as skin, to reach cancer cells inside the bodies.⁸⁻¹⁰ On the other hand, photoluminescence quantum yield is an important figure for bioimaging applications.¹¹⁻¹² As a result, the studies of the optical properties of various QDs have gained increasing attentions. The optical properties of QDs are different from their respective bulk materials due to significant quantum confinement in all spatial dimensions.¹³ The band gap increases due to the confined electron waves, which affect both the optical absorption and photoluminescence wavelength to a large extent. Therefore, it is of great scientific interest to investigate the optical properties of various QDs so as to pave the way for the potential biomedical applications.

In this work, tellurium quantum dots (TeQDs) were prepared by ultrasonic ablation of Te bulk powder and dispersed in solvent. After purification, X-ray diffraction (XRD), transmission electron microscopy (TEM), scanning electron microscope (SEM) and atomic force microscopy (AFM) were used to study the structural and morphological properties, X-ray photoelectron microscopy (XPS) and energy dispersive spectroscopy (EDS) were used to investigate the chemical composition and bonding. This was followed by systematic determination of the optical properties of the TeQDs to investigate their optical absorption and PL.

3. Experimental

Materials

Te powder (99.999%) and 1-Methyl-2-pyrrolidone (NMP) were purchased from Sinopharm Chemical Reagent Co., Ltd. All chemicals were used as received without further purifications.

Preparation of TeQDs

0.5 g of Te powder was grinded into fine powder in an agate mortar, and was then transferred into a beaker and 50 ml of NMP was added. The solution was sonicated for 4 h in an ultrasonic bath at room temperature. The resultant dark brown suspension was centrifuged at 2000 rpm for 15 min. The clear and brown-colored supernatant was collected as TeQDs solution.

Characterization of TeQDs

The morphology, size distribution and crystal structure of the TeQDs were investigated using TEM (Tecnai G2 TF30 S-Twin). The diameter of the TeQDs was further confirmed with AFM (Seiko SPA 400). The XRD (Ultima IV, X-ray source: Cu K α , λ = 0.154178 nm) of TeQDs was performed to compare with bulk Te to ensure the structural integrity of TeQDs after ultrasound treatment. The chemical bonding was analyzed by XPS (PHI Versa probe II) using 50W Al K α radiation. Optical absorption was performed using a UV-Vis spectrometer (Shimadzu UV-3600). PL measurements were carried out with a fluorescent spectrometer (Hitachi, F-4500).

4. Results and Discussion

The lattice of tellurium is a long chain structure. The atoms are covalently bonded to form a long helical chains that are spatially arranged in parallel through the van der Waals effect. Due to the weak van der Waals forces, TeQDs were obtained after grinding, ultrasonic treatment and centrifugation of the Te powder. Figure 1(a) shows the TeQDs dispersed in the solution.

Figure 1(b) shows the TEM image of the TeQDs. The TeQDs have a dot-like shape and diameter below 10 nm. The TeQDs have a narrow size distribution ranging from 3 to 5 nm as shown in Figure 1(c). It fits well with a Gaussian distribution (red line) which implied that the TeQDs formed a mono-dispersion. The fitting parameters indicated that the average diameter of TeQDs was 4.10 nm with a small FWHM of 0.9 nm. The good crystallinity of the TeQDs was revealed in the high resolution TEM (HR-TEM) image shown in Figure 1(d).¹⁴ The lattice fringes was clearly identified with a lattice interplanar distance of 0.172 nm as seen from the line profile (blue line) in Figure 1(e), which corresponded to the (102) plane of tellurium. The SEM image of the TeQDs film formed from repeated drop-casting of TeQD solution followed by solvent evaporation is shown in Figure 1(f). EDS performed on the film as shown in Figure 1(g) revealed that the atomic ratio of C/N/O/Te was 26.4/6.9/26.2/40.5 (%). The C, N and O could originate from the NMP solvent adsorbing water molecules from air which possibly indicated the oxidation of TeQDs to TeO₂ by oxygen from the air, as reported by Garbassi *et al.*¹⁵

Figure 1(i) shows the XRD pattern of the TeQDs film. The peaks at $2\theta = 27.56^\circ$, 38.26° and 40.41° corresponded to the (101), (102) and (110) lattice planes of tellurium, respectively. The peak of (101) has the largest intensity and represents a d -spacing of 0.323 nm (Figure 1(h)). The XRD pattern was in good agreement with the trigonal tellurium (*t*-Te). The average particle size in the TeQDs film was calculated using the Debye-Scherrer equation:

$$D = 0.89\lambda/(\beta\cos\theta) \quad (1)$$

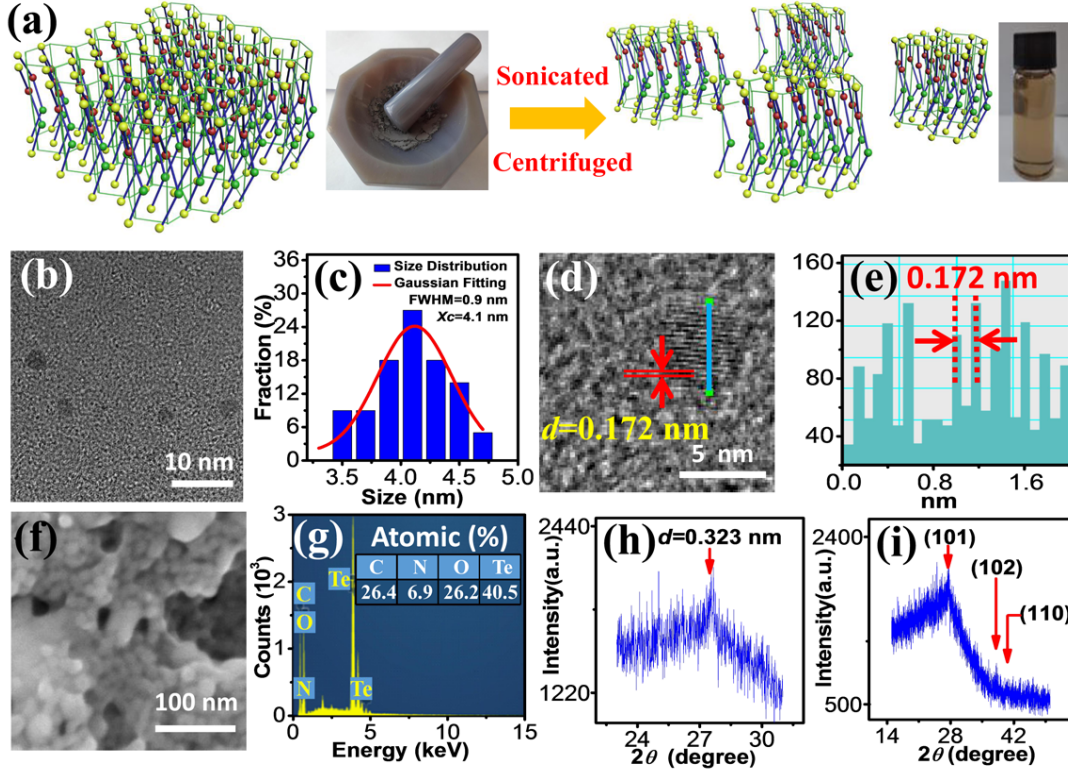


FIG.1. (a) The schematic illustration of the preparation of TeQDs. (b) TEM image of TeQDs. (c) Particle size distribution of TeQDs from TEM. (d) The HR-TEM image of one TeQD. (e) The line profile analysis of TeQD. (f) The SEM image of TeQDs film. (g) The EDS analysis of the TeQDs film. (h) The XRD diffraction pattern of TeQDs. (i) The full scan XRD diffraction pattern of the TeQDs

where D is the average particle size, λ is the X-ray wavelength, β and θ are the FWHM ($= 0.357$ nm) and diffraction angle of the (101) peak, respectively. The average particle size obtained from the above equation was 3.96 nm, which is consistent with the average size of TeQDs observed from the TEM measurement.

AFM measurement was also performed to determine the size of the TeQDs. The AFM image of the TeQDs is shown in Figure 2(a). The height profiles of three TeQDs labeled with A, B and C are shown in Figure 2(b) and their heights were 4.05, 3.95 and 3.88 nm respectively, with an average height of 3.96 nm. This was consistent with the TEM and XRD measurements.

The bandgap energy (E_g) of TeQDs was calculated using the Eq. (2)¹⁶

$$E_g \approx E_{g(0)} + \frac{\hbar^2 \pi^2}{2\mu R^2} - \frac{1.78e^2}{\epsilon R} \quad (2)$$

Where $E_{g(0)}$ is the bandgap of bulk Te (0.35 eV)¹⁷, \hbar ($\hbar = h/(2\pi)$) is the reduced Planck constant, e is the electron charge, μ ($\mu = [\frac{1}{m_{e^-}} + \frac{1}{m_{h^+}}]^{-1}$) is the

reduced mass of the electron and hole in the quantum region, ϵ ($\epsilon = 5$) is the dielectric constant of Te, R (2 nm) is the radius of TeQD. The calculated E_g is 1.34 eV which is much bigger than the bulk value (0.35 eV)¹⁷ due to quantum effect.

The crystal structure of the TeQDs was investigated using fast Fourier transform (FFT) (see inset of Figure 2(c)) performed on the TeQDs indicated by a red square in Figure 2(c). The FFT image showed that the TeQDs have a hexagonal crystal structure which was similar to the bulk tellurium. The hexagon in the FFT image was slightly tilted, which corresponded to the trigonal tellurium.

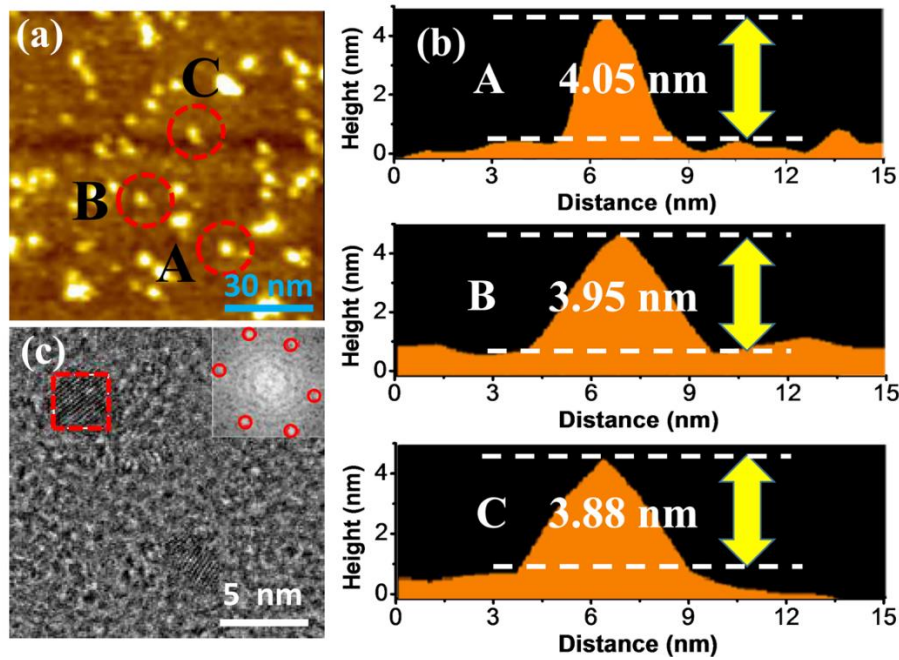


FIG.2. (a) AFM image of the TeQDs. (b) The height analysis of location A, B and C indicated in (a). (c) The HR-TEM image of the TeQDs, inset: the Fast Fourier Transform (FFT) of the selected TeQD.

Figure 3(a) shows the Raman spectrum of the TeQDs. Two peaks appeared at 122.6 and 142.2 cm^{-1} , which could be attributed to the Te-Te bond vibration modes.¹⁸ When compared with the peak positions of 121.0 and 140.8 cm^{-1} reported for bulk tellurium by Vinod *et al.*,¹⁸ the observed peaks for TeQDs were right-shifted by 1.6 and 1.4 cm^{-1} respectively, which might indicate the presence of stress in the lattice of the TeQDs.¹⁹ The shift towards higher frequencies could be related to the surface effect. As the diameter of the tellurium reduces, the surface area and surface energy would increase drastically.

The XPS spectrum of the TeQDs is presented in Figure 3(b). The three strongest peaks located at 283.2, 574.5 and 583.8 eV were assigned to the C 1s, Te 3d_{5/2} and Te 3d_{3/2} respectively. Two smaller peaks at 398 and 530 eV were the N 1s and O 1s peaks

respectively. The peaks marked with red arrows, such as the C 1s, N 1s and O 1s peaks, were attributed to the NMP solvent and possible oxidation of Te forming TeO₂, as previously discussed. The two Te-related peaks, as shown in Figure 3(c), were the Te 3d_{5/2} and Te 3d_{3/2} peaks. They were due to the spin-orbit coupling that led to a split of the Te 3d orbital.²⁰

Figure 4(a) shows the UV-Vis absorption spectrum of the TeQD solution. The solution was gradually diluted in order to observe the absorption peak more clearly. An absorption peak was observed at 288 nm. The inset in Figure 4(a) shows the photograph of the TeQD solution under ambient light (left) and ultraviolet light illumination (right).

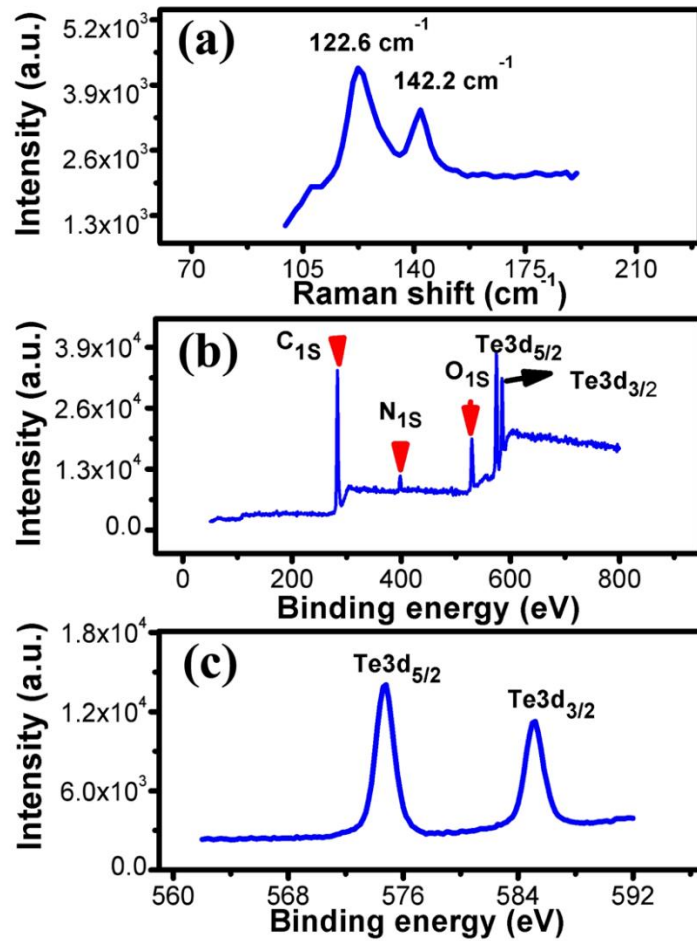


FIG.3. (a) The Raman spectrum of the TeQDs. (b) The XPS spectrum of the TeQDs (c) The Te 3d_{5/2} and Te 3d_{3/2} XPS spectrum.

The bandgap energy (E_g) of TeQDs can also be obtained by Tauc plot using Eq. (3),

$$\alpha hv = A(hv - E_g)^{1/2} \quad (3)$$

where α is the absorption coefficient, A is a constant, $h\nu$ is the photo energy, E_g is the bandgap energy. The bandgap energy of TeQDs²¹ may be estimated from the curve of the $(\alpha h\nu)^2$ vs. photo energy ($h\nu$), the estimated value is 1.32 eV (as shown in Fig. S1 in the supplementary material) which is very near to that calculated from quantum size effect (1.34 eV) using Eq. (2).

The photoluminescence (PL) spectra of the TeQD solution are shown in Figure 4(b). The excitation wavelength was varied from 300 to 500 nm, in 20 nm steps. The excitation wavelength covered the range from UV to visible light. The PL emission of the TeQDs was basically within the visible light region between blue to green emission. As the excitation wavelength red-shifted, the emission peak also red-shifted, thus the TeQD solution exhibited excitation-wavelength-dependent emission, which was commonly observed in other QD solutions such as the graphene QDs.²⁰ The emission light energy is smaller than the excited energy which is due to the vibration relaxation caused by Stokes shift²². The photoluminescence excitation (PLE) spectra are shown in Figure 4(c). The peak marked with a star was due to the PLE system and not the sample. The emission intensity was monitored from 380 to 500 nm, in 20 nm

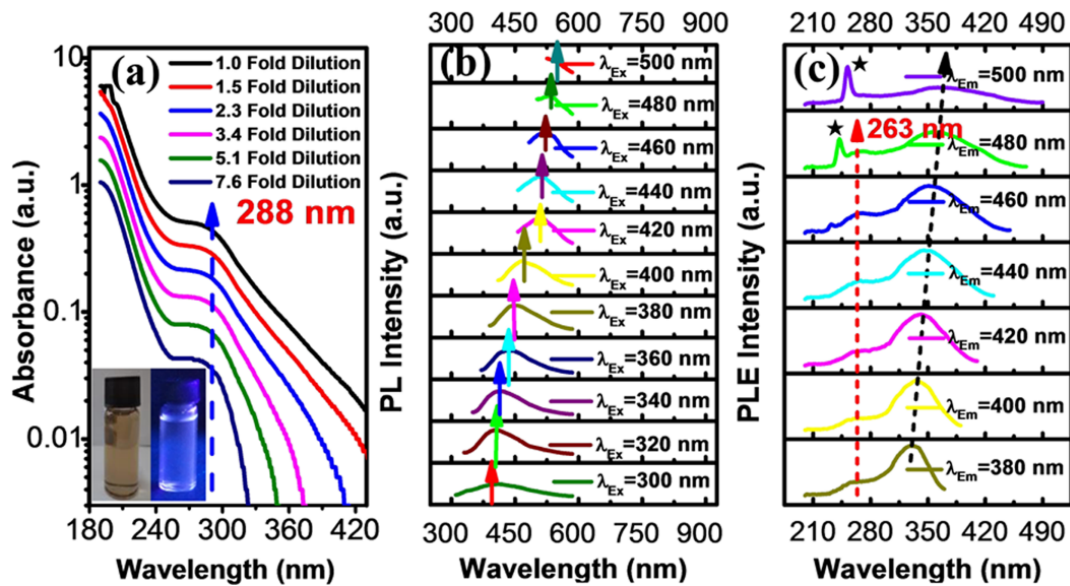


FIG.4. (a) The UV-Vis absorption spectra of the TeQDs with different folds of dilution. (b) PL spectra of the TeQDs with excitation wavelengths ranging from 300 to 500 nm. (c) PLE spectra of the TeQDs recorded as a function of emission wavelength ranging from 380 to 500 nm.

steps. Similar to the PL emission spectra, the maximum PLE peak also red-shifted as the emission wavelength red-shifted. This is indicated with a black arrow. However, the peak at 263 nm did not shift with the emission wavelength as depicted by the red arrow. Based on the study of structure and optical properties, the energy level

structure has been proposed (as shown in Fig. S2 in the supplementary material), only those photons energies that match specific energy level differences can be absorbed.²² It is proposed that TeQDs contains multiple energy levels due to the quantum-size, which facilitates some electron transition pathways, leading to the red-shift of PL.

To investigate the wavelength-dependent PLE and PL peaks in greater details, the normalized PLE and PL spectra are shown in Figure 5(a) and 5(b) respectively. As the monitored emission wavelength (PLE) was red-shifted by 120 nm (Figure 5(a)), the excitation wavelength that produced maximum emission (*i.e.* the PLE peak) also red-shifted by 43 nm. As the excitation wavelength red-shifted by 200 nm (Figure 5(b)), the emission wavelength (PL) also red-shifted by 151 nm. It was found that both the energy-dependence PLE and PL peaks followed closely a linear relationship as shown in Figure 5(c). The linear dependence of PLE and PL peaks on energy enables multicolour emission properties which enriches a variety of PL emission colours of TeQDs.

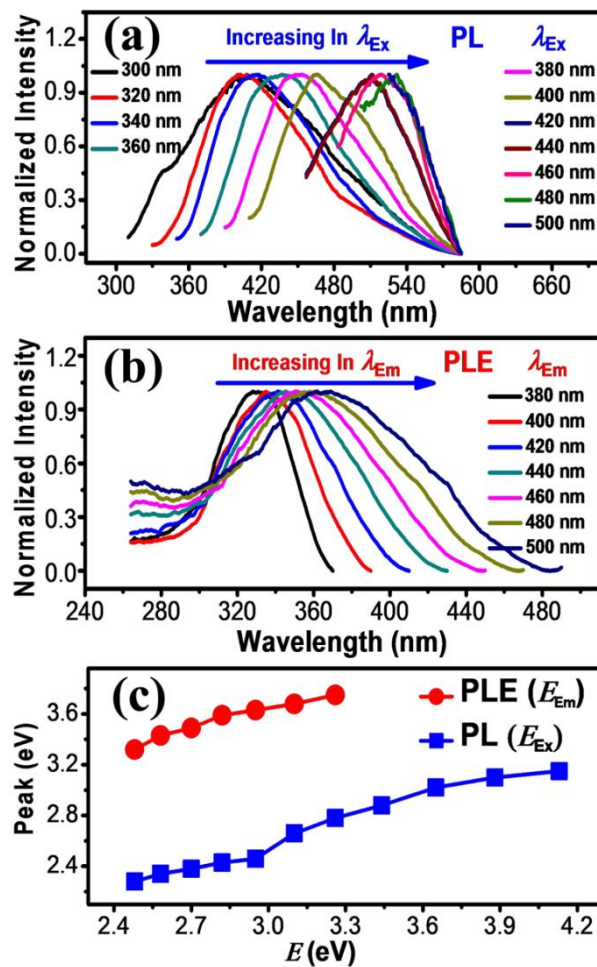


FIG. 5. (a) Normalized PL spectra of the TeQDs excited by various wavelengths ranging from 300 to 500 nm in 20 nm steps. (b) Normalized PLE spectra of the TeQDs. (c) The linear relationship between the peak excitation energy (PLE peak) and emission energy (E_{Em} , red line) and the linear relationship between the emission peak energy (PL peak) and excitation energy (E_{Ex} , blue line).

5. Conclusion

Tellurium quantum dots (TeQDs) with an average diameter of 4 nm were prepared by ultrasonic ablation of Te bulk powder. The as-prepared TeQDs have a narrow size distribution. Optical properties of the TeQDs including absorption and PL were investigated. The TeQDs absorbed strongly in the UV region and the PL emission was in the visible light region with a wavelength tunable from blue to green color by changing the excitation wavelength from 300 to 500 nm. The TeQDs have potential applications in photothermal therapy and bioimaging, however its biocompatibility required further investigation.

See supplementary material for the Tauc plot (supplementary Fig. S1) and energy level diagram of TeQDs (supplementary Fig. S2).

Acknowledgements

This work was supported by National Natural Science Foundation of China (No. 51462037 and No. 61106098), and the Key Project of Applied Basic Research of Yunnan Province, China (No. 2012FA003).

References

- ¹R. Gui, H. Jin, Z. Wang, and L. Tan, *Coord. Chem. Rev.* **269**, 91 (2015).
- ²M. Chu, X. Pan, D. Zhang, Q. Wu, J. Peng, and W. Hai, *Biomaterials* **33**, 7071 (2012).
- ³M. Werwie, N. Fehr, X. Xu, T. Basché, and H. Paulsen, *Biochim. Biophys. Acta* **1840**, 1651 (2014).
- ⁴E. V. Shashkov, M. Everts, M. E. I. Galanzha, and V. P. Zharov, *Nano Lett.* **27**, 3953 (2008).
- ⁵S. V. Kershaw, A. S. Susha, and A. L. Rogach, *Chem. Soc. Rev.* **42**, 3033 (2013).
- ⁶J. Z. Zhang, J. K. Cooper, and S. Gul, *J. Phys. Chem. Lett.* **5**, 3694 (2014).
- ⁷C. S. S. Sandeep, J. M. Azpiroz, W. H. Evers, S. C. Boehme, I. Moreels, S. Kinge, L. D. A. Siebbeles, I. Infante, and A. J. Houtepen, *ACS Nano* **8**, 11499 (2014).
- ⁸B. del Rosal, E. Carrasco, F. Ren, A. Benayas, F. Vertrone, F. Sanz-Rodríguez, D. Ma, Á. Juarranz, and D. Jaque, *Adv. Funct. Mater.* **26**, 6060 (2016).
- ⁹A. Benayas, F. Ren, E. Carrasco, V. Marzal, B. del Rosal, B. A. Gonfa, Á. Juarranz, F. Sanz-Rodríguez, D. Jaque, J. Garía-Solé, D. Ma, and F. Vetrone, *Adv. Funct. Mater.* **25**, 6650 (2016).
- ¹⁰Y. Yong, X. Cheng, T. Bao, M. Zu, L. Yan, W. Yin, C. Ge, D. Wang, Z. Gu, and Y. Zhao, *ACS Nano* **9**, 12451 (2015).

- ¹¹Z. Fan, Y. Li, X. Li, L. Fan, S. Zhou, D. Fang, and S. Yang, *Carbon* **70**, 149 (2014).
- ¹²L. Lin, Y. Xu, S. Zhang, I. M. Ross, A. C. M. Ong, and D. A. Allwood, *ACS Nano* **7**, 8214 (2013).
- ¹³C. Dong, X. Li, and J. Qi, *Phys. Chem. Chem. Phys.* **13**, 14467 (2011).
- ¹⁴Y. Wang, K. Yang, H. Pan, S. Liu, X. Xu, and L. Zhou, *Chem. J. Chin. U.* **12**, 2604 (2012).
- ¹⁵F. Garbassi, J. C. J. Bart, and G. Petrini, *J. Electron. Spectrosc. Relat. Phenom.* **22**, 95 (1981).
- ¹⁶N. Satoh, T. Nakashima, K. Kamikura, and K. Yamamoto, *Nat. Nanotech.* **2**, 106 (2008).
- ¹⁷Z. H. Lin, Z. Yang, and H. T. Chang, *Cryst. Growth Des.* **1**, 351 (2008).
- ¹⁸E. M. Vinod, A. K. Singh, R. Ganesan, and K. S. Sangunni, *J. Alloys Compd.* **537**, 127 (2012).
- ¹⁹G. Lucovsky, *Phys. Stat. Sol.* **49**, 633 (1972).
- ²⁰X. Li, S. Lau, L. Tang, R. Ji, and P. Yang, *Nanoscale* **6**, 5323 (2014).
- ²¹L. Ma, W. H. Li, and J. H. Luo, *Mater. Lett.* **13**, 65 (2013).
- ²²X. Li, S. Lau, L. Tang, R. Ji, and P. Yang, *J. Mater. Chem. C* **1**, 7308 (2013).